A&A, 709, A48 (2026)
https://doi.org/10.1051/0004-6361/202557755

Astronomy & Astrophysics

The complex relationships between active galactic nuclei, bars, and bulges

I. L. Garland[1,2,⋆], H. Best[1], L. F. Fortson[3,4], T. Géron[5], C. J. Lintott[6], D. O'Ryan[7], B. D. Simmons[2], R. J. Smethurst[6], M. Viskotová[1], M. Walmsley[5,8], N. Werner[1], and M. Zajaček[1]

[1] Department of Theoretical Physics and Astrophysics, Faculty of Science, Masaryk University, Kotlářská 2, Brno 611 37, Czech Republic
[2] Department of Physics, Lancaster University, Lancaster LA1 4YB, UK
[3] School of Physics and Astronomy, University of Minnesota, Minneapolis, Minnesota 55455, USA
[4] Minnesota Institute for Astrophysics, University of Minnesota, Minneapolis, Minnesota 55455, USA
[5] Dunlap Institute for Astronomy and Astrophysics, University of Toronto, 50 St. George Street, Toronto, ON M5S 3H4, Canada
[6] Oxford Astrophysics, Department of Physics, University of Oxford, Denys Wilkinson Building, Keble Road, Oxford OX1 3RH, UK
[7] European Space Agency (ESA), European Space Astronomy Centre (ESAC), Camino Bajo del Castillo s/n, 28692 Villaneuva de la Cañada, Madrid, Spain
[8] Jodrell Bank Centre for Astrophysics, Department of Physics & Astronomy, University of Manchester, Oxford Road, Manchester M13 9PL, UK

Received 20 October 2025 / Accepted 28 March 2026

ABSTRACT

Context. Via scaling relations, it is well known that active galactic nuclei (AGNs) and bulges are linked. This link was thought to be driven by mergers, but recent studies show that secular processes are the dominant mechanism of supermassive black hole growth. One such secular mechanism is gas inflow driven by large-scale bars. Since bulges can also grow via these bars, these three features likely share some common process.
Aims. We investigated whether the observed correlation between AGNs and bars is real or arises as a result of correlations between bars and bulges.
Methods. Using a catalogue of AGN identifications and galaxy morphologies in the DESI Legacy Survey at $z \leq 0.1$, we controlled for mass and colour and investigated the AGN fraction variation with bulge prominence and bar strength.
Results. We first show that the variation in the AGN fraction between strongly barred, weakly barred, and unbarred galaxies does not qualitatively change if we additionally control for bulge prominence. Second, we find that in fixed bins of bulge prominence, the AGN fraction increases with increasing bar strength. In subsamples split by bar strength, the AGN fraction increases with bulge prominence, indicating that AGN presence correlates with bar strength and bulge prominence simultaneously.

Key words. galaxies: active – galaxies: bulges – galaxies: evolution – galaxies: structure

1. Introduction

The co-evolution of supermassive black holes (SMBHs) with their host galaxies is observed through a number of scaling relations (see Fabian 2012; Kormendy & Ho 2013; Heckman & Best 2014, for a review). SMBH masses have been found to correlate with both bulge properties, such as velocity dispersion and bulge stellar mass (Ferrarese & Merritt 2000; Häring & Rix 2004; Beifiori et al. 2012), and properties of the host galaxy as a whole, such as total stellar mass (Cisternas et al. 2011; Marleau et al. 2013; Simmons et al. 2017).

Supermassive black holes gain most of their mass during periods of rapid growth and accretion, during which they are observed as active galactic nuclei (AGNs; Shlosman et al. 1989). Therefore, by examining AGNs, we can investigate the origins of this co-evolution between SMBHs and their host galaxies.

Whilst mergers between two or more galaxies are known to be one source of AGN triggering (e.g. Urrutia et al. 2008; Glikman et al. 2015), simulations have shown that most SMBH growth occurs via secular (i.e. merger-free) pathways (Martin et al. 2018; McAlpine et al. 2020; Smethurst et al. 2024). However, obtaining a pure and complete sample of galaxies with no major mergers in their recent history is highly challenging observationally.

Martig et al. (2012) showed that galaxies with a bulge–to–total mass ratio of less than 0.1 (i.e. little to no bulge) have had no mergers with a mass ratio greater than 1:4 since $z \sim 2$. Thus, we could select bulge-less galaxies as a merger-free sample. However, this sample would be incomplete since pseudo-bulges grow in the absence of mergers (Kormendy & Kennicutt 2004; Kormendy et al. 2010). They look morphologically very similar to classical bulges, and without careful structural decomposition combined with dynamical analysis (such as via the Kormendy relation; Kormendy 1977; Hamabe & Kormendy 1987), distinguishing between secularly built pseudo-bulges and merger-built classical bulges is virtually impossible, and significant cross-contamination between bulge types is common. Additionally, there is substantial evidence that merger-free formations of classical bulges are possible (Parry et al. 2009; Bell et al. 2017; Gargiulo et al. 2017; Park et al. 2019; Wang et al. 2019; Guo et al. 2020; Du et al. 2021), for example through disk instabilities. Thus,

⋆ Corresponding author: garland@mail.muni.cz

removing all galaxies with a bulge from a sample could mean removing a large number of secularly grown bulges.

Simmons et al. (2017) used a sample of disk-dominated galaxies, without distinguishing the components of pseudo-bulges and classical bulges, and show that galaxy stellar mass correlates well with black hole mass in disk galaxies, better than bulge stellar mass. This sample was later confirmed via careful structural decomposition and use of the Kormendy relation; classical bulges were found in 53% of the galaxies and pseudo-bulges in 64%, with some galaxies containing both a classical and a pseudo-bulge component (Fahey et al. 2025).

The other crucial complication that arises when removing galaxies with a bulge component from a sample is that large-scale galactic bars can build up pseudo-bulges, providing a correlation between bar presence and bulge presence (Shlosman et al. 1989; Kormendy & Kennicutt 2004; Laurikainen et al. 2007; Combes 2009). Therefore, removing all galaxies with a bulge component would affect any observed relationship between bars and AGNs.

A correlation between AGN presence and bar presence has been found in a number of works (Knapen et al. 2000; Laine et al. 2002; Laurikainen et al. 2004; Coelho & Gadotti 2011; Oh et al. 2012; Alonso et al. 2018; Garland et al. 2023; Kataria & Vivek 2024; La Marca et al. 2026). However, due to the challenges in separating AGN emission from that of the host galaxy, along with the rarity of observationally merger-free disks (those with only a small bulge component) and the rarity of AGNs, many of these studies find only a tenuous link, with high levels of uncertainty. Other studies find no link at all (e.g. Cheung et al. 2015; Goulding et al. 2017). Some studies (e.g. Galloway et al. 2015; Silva-Lima et al. 2022) find a higher AGN fraction in barred galaxies, but not higher levels of AGN activity, as measured by the [O III] luminosity. Garland et al. (2024) included all disk galaxies, regardless of their bulge size, and looked at the AGN fraction with bar strength (divided into unbarred, strongly barred, and weakly barred categories using Galaxy Zoo DESI machine-learning predicted volunteer votes) across the disk-dominated galaxy population. In doing so, they show to a $>5\sigma$ confidence that strongly barred galaxies are more likely to host AGNs than weakly barred galaxies, which are in turn more likely to host AGNs than unbarred galaxies.

In this work we investigated whether AGN presence correlates exclusively with bulge presence, or whether AGN presence is linked with both bars and bulges in some way. We divided a sample of disk-dominated galaxies by bulge prominence (using Galaxy Zoo DESI), and investigated the AGN fraction in strongly barred, weakly barred, and unbarred galaxies at each bulge prominence. This allowed us to test the AGN–bulge link at the same time as the AGN–bar link. Since we do not have high-quality photometric decomposition, nor measurements like the surface brightness of each morphology component, we do not distinguish between classical and pseudo-bulges in this work.

In Sect. 2 we discuss the sample selection. Our results are presented in Sect. 3, followed by a discussion and our conclusions in Sects. 4 and 5. Throughout this work, we used WMAP9 cosmology (Hinshaw et al. 2013) and assumed a flat Universe, with $H_0 = 69.3\,\mathrm{km\,s^{-1}\,Mpc^{-1}}$ and $\Omega_\mathrm{m} = 0.287$, implemented via ASTROPY (Astropy Collaboration 2013, 2018, 2022).

2. Sample selection

To study the combined effect of galactic bulges and bars on AGN presence, we utilised the Galaxy Zoo: DESI (GZD) catalogue (Walmsley et al. 2023b). GZD consists of morphology classifications for 8.7 million galaxies in the DESI Dark Energy Spectroscopic Instrument Legacy Surveys (DESI-LS), made with *Zoobot*, a neural network trained on Galaxy Zoo volunteer votes (Walmsley et al. 2023a).

In brief, DESI-LS consists of galaxies observed as part of DECaLS, BASS, and MzLS[1]. Given the resulting size of DESI-LS, volunteer votes alone (as in previous Galaxy Zoo campaigns such as Galaxy Zoo 2 and Galaxy Zoo Hubble) are not efficient enough, and would take too long to collect for the entire catalogue. Thus, volunteer votes on a subset of the data (401k galaxies) are used to train *Zoobot*. We refer the reader to the release paper for a detailed description of the initial catalogue (Walmsley et al. 2023a).

To obtain the morphology and ionisation source classifications, we used the catalogue compiled in Garland et al. (2024, hereafter G24). We refer the reader to their paper for a detailed description, but we summarise it in brief here.

Walmsley et al. (2023b) matched GZD to the MPA-JHU SDSS DR7[2] catalogue (Abazajian et al. 2009) with a 3 arcsec radius to obtain emission line fluxes, stellar masses, and colours (Kauffmann et al. 2003; Salim et al. 2007). G24 matched GZD to NYU-VAGC to obtain k-corrections (Blanton et al. 2005), also within a 3 arcsec radius.

To select a sample of not-edge-on, not-merging disks, G24 used the GZD model-predicted vote fractions. To select a sample of disks, G24 selected galaxies with $f_\mathrm{smooth-or-featured\_featured-or-disk} \geq 0.27$, where $f_\mathrm{smooth-or-featured\_featured-or-disk}$ is the fraction of volunteers who voted for 'featured or disk', as predicted by *Zoobot*. The cutoff value was recommended by Walmsley et al. (2022). To select disks that are not edge-on, G24 again followed the procedure in Walmsley et al. (2022) and selected galaxies with $f_\mathrm{disk-edge-on\_no} \geq 0.68$, where $f_\mathrm{disk-edge-on\_no}$ is the model-predicted fraction of volunteers who voted for 'not edge-on'. To select merger-free galaxies, G24 defined a new parameter of merger-prominence, ζ_avg, which combines the vote fractions for each category that volunteers can select – 'merging', 'major disturbance', 'minor disturbance', or 'none'. They identified $\zeta_\mathrm{avg} < 0.3$ as the ideal cutoff vote fraction to select merger-free galaxies in order to maximise both completeness and purity. The first two conditions are described in Walmsley et al. (2022), and merger prominence in G24. We wanted not-edge-on galaxies since this makes bars (where present) easier to see, and whilst bars can sometimes be detected in edge-on galaxies, there is likely to be a bias present when asking volunteers to classify galaxies. Thus, to ensure we removed this potential bias, we limited our sample to not-edge-on disks.

Having compiled the initial sample, G24 separated the galaxies into unbarred, weakly barred, and strongly barred categories. Using the methodology in Géron et al. (2021), a galaxy is designated as unbarred (UBAR) if $f_\mathrm{strong-bar} + f_\mathrm{weak-bar} < 0.5$, where $f_\mathrm{x-bar}$ is the model-predicted vote fraction for that bar strength. Otherwise, it is considered barred. This barred sample was then further split into strong and weak. A galaxy is designated as weakly barred (WBAR) if it is not unbarred and $f_\mathrm{strong-bar} < f_\mathrm{weak-bar}$. A galaxy is designated as strongly barred (SBAR) if it is not unbarred and $f_\mathrm{strong-bar} \geq f_\mathrm{weak-bar}$. To ensure completeness and reduce selection effects, G24 volume-limited the

[1] Dark Energy Camera Legacy Survey, Beijing-Arizona Sky Survey, and Mayall z-band Legacy Survey, respectively.
[2] Sloan Digital Sky Survey Data Release 7.

sample, with redshift $z \leq 0.1$ and r-band absolute magnitude $M_r \leq -19.2$, as shown in their Fig. 1.

Additionally, for this work we required an estimate of the bulge contribution to the galaxy morphology, which we refer to as the bulge prominence. Masters et al. (2019) defined a bulge prominence parameter, $B_{\rm avg}$, using SDSS morphology classifications from Galaxy Zoo 2 (GZ2; Willett et al. 2013). However, GZ2 had only four different categories of bulge presence: none, just noticeable, obvious, and dominant. GZD divides bulge presence into five categories: none, small, moderate, large, and dominant. Thus, we adapted $B_{\rm avg}$ to

$$B = 0.25 f_{\rm small} + 0.5 f_{\rm moderate} + 0.75 f_{\rm large} + 1.0 f_{\rm dominant}, \quad (1)$$

where B is the bulge prominence parameter used in this work, and f_x is the fraction of volunteers who voted for the bulge category (x) as predicted by *Zoobot*.

Note that there is no specific reason for these exact coefficients, as the aim is simply to condense the bulge vote fractions into one numeric parameter. To confirm this, we tested several combinations of coefficients, and our results and analysis do not qualitatively change for any reasonable choice of coefficient weights on the different vote fractions.

As with any measurement, the GZD vote fractions do have errors associated with them. When the vote fractions are varied within their errors (assumed to be Gaussian) using a bootstrapping method iterated 1000 times with replacements, our results do not qualitatively change.

G24 also published classifications of the ionisation source. The authors divided their sample via emission-line diagrams (Baldwin et al. 1981; Veilleux & Osterbrock 1987; Rosario et al. 2016) into AGN, star-forming, low-ionisation nuclear emission-line region (LINER), composite, undetermined, and uncertain galaxies. The undetermined galaxies are those that have Hα flux with a signal-to-noise ratio ($S/N_{H\alpha}$) of <3 and thus have neither sufficient star-formation nor AGN activity to make an accurate determination. Visual inspection shows that these undetermined galaxies (in this disk-dominated sample) are predominantly quiescent, red spirals. Uncertain galaxies are those that lack sufficient signal-to-noise in other utilised emission lines (Hβ, [O III], [N II], [S II], and [O I]) such that they could theoretically fall into multiple other categories. We removed from our sample uncertain galaxies (since their ionisation source remains unknown), composite galaxies (since the split between how much ionisation results from AGNs compared to star formation is unknown), and LINERs (since it remains debated whether they are low-luminosity AGN or highly star-forming galaxies). Again, we refer the reader to G24 for a full description of the ionisation classification procedure, notably their Fig. 2.

These cuts to the data resulted in our final volume-limited sample of 32 683 disk-dominated, not edge-on, not-merging galaxies that are either AGN, star-forming, or undetermined. There are 20 417 unbarred, 9166 weakly barred, and 3100 strongly barred galaxies. There are 3164 AGN hosts, 28 807 star-forming galaxies, and 712 undetermined galaxies. The median bulge prominence is 0.34, with a mean of 0.36 and a standard deviation of 0.07.

3. Results

We first looked at the spread of parameters thought to correlate with bar presence and AGN presence: stellar mass, k-corrected $(g-r)_0$ colour (where the 0 indicates correction for Galactic absorption), and bulge prominence. The stellar masses and colours were taken from SDSS DR7, which had stellar mass errors of the order of $\Delta \log(M_*/M_\odot) \pm 0.1$. The distributions are shown in Fig. 1 for AGN, star-forming, and undetermined sources, and in Fig. A.1 for LINER, composite, and uncertain sources, since we do not directly use the latter three in this work.

Table 1. Percentage of each ionisation category within each bar classification, as shown in Fig. 2.

		UBAR	WBAR	SBAR
This work	AGN	15.9 ± 0.7	22.5 ± 0.8	27.6 ± 0.8
	SFing	81.9 ± 0.7	74.2 ± 0.8	68.2 ± 0.9
	Undet	2.2 ± 0.3	3.3 ± 0.4	4.2 ± 0.4
G24	AGN	14.2 ± 0.6	23.3 ± 0.8	31.6 ± 0.9
	SFing	83.9 ± 0.6	73.6 ± 0.8	63.6 ± 0.9
	Undet	1.9 ± 0.2	3.1 ± 0.3	4.7 ± 0.4

Notes. UBAR is unbarred galaxies, WBAR is weakly barred, and SBAR is strongly barred. We show the results from G24 for comparison. AGN presence in strongly barred galaxies is around twice as prolific as in unbarred galaxies.

It is worth noting that the smallest bulge prominences (i.e. the low-bulge-prominence end of the histogram) in the AGN and inactive (star-forming and undetermined) subsamples are very similar. One might expect a higher minimum bulge prominence in the AGN subsample if AGNs get mistaken for a bulge component during visual classifications. Hence, we can be reassured that AGN-host galaxies are not mistakenly being classified as bulge galaxies.

To account for the difference in M_*, $(g-r)_0$ and B, we controlled for these three parameters by weighting our sample. We divided our sample into ten evenly spaced bins in each parameter, with cuts on the high and low ends of each parameter in order to remove outliers. These cuts are

- $5.0 \leq \log(M_*/M_\odot) \leq 12.0$.
- $-0.2 \leq (g-r)_0 \leq 2.0$.
- $0 \leq B \leq 1.0$.

Given that we are dividing each parameter into ten bins, this gives us a total of 1000 bins.

From here, in each bin we assigned weights to each galaxy such that the weighted distributions of these three parameters are the same between the SBAR, WBAR, and UBAR subsamples. This means that our results with the weighted sample will not be affected by the mass, colour, or bulge prominence. This extends the work of G24, who only controlled for M_* and $(g-r)_0$.

We looked at the overall AGN fraction ($f_{\rm AGN}$) in each of the bar subsamples. These results are shown in Fig. 2 and Table 1. After controlling for M_*, $(g-r)_0$ and B, the AGN fraction in strongly barred galaxies is greater than that in weakly barred galaxies, which is greater than in unbarred galaxies, to a $>3\sigma$ confidence.

Whilst the overall trends agree with those of G24, the quantitative results differ slightly. When controlling for bulge prominence, the AGN fraction still increases with bar strength, with a $>3\sigma$ difference between $f_{\rm AGN,SBAR}$, $f_{\rm AGN,WBAR}$, and $f_{\rm AGN,UBAR}$. The quantitative values are in agreement with G24 to 3σ for the WBAR and UBAR AGN fractions, but for SBAR, the AGN fraction is lower and the star-forming fraction is higher. This implies that some of the observed difference in the AGN fraction between strong and weakly barred galaxies is due to the bulge, but only a minor part of the difference. Even when controlling for bulge presence, the AGN fraction still increases with bar strength, as in G24.

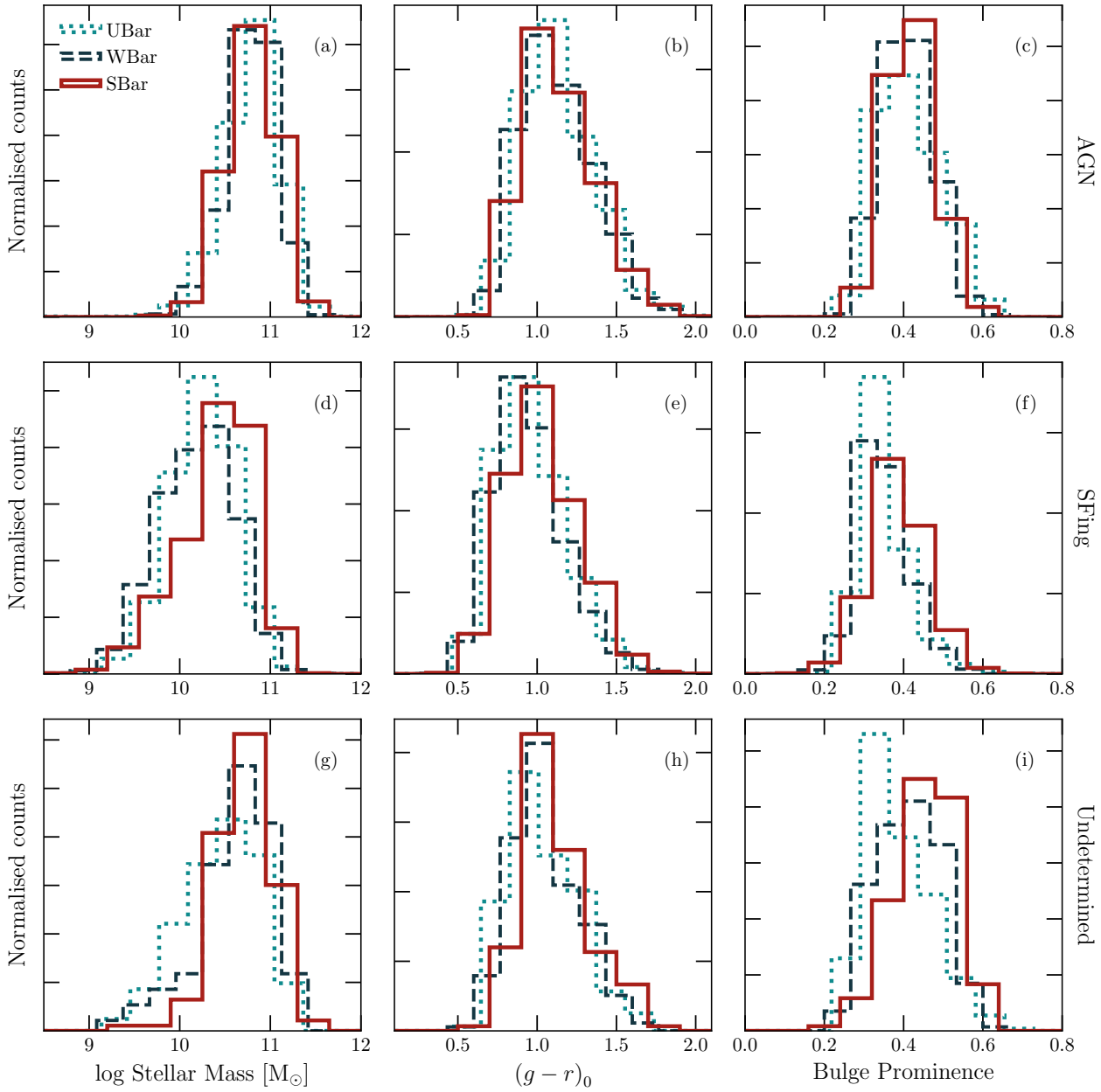

Fig. 1. Distributions of stellar mass (left column), $(g-r)_0$ colour (middle column), and bulge prominence (right column) for AGNs (top row), star-forming galaxies (middle row), and undetermined galaxies (bottom row). We show strongly barred galaxies in solid red lines, weakly barred in dashed navy blue, and unbarred in dotted teal. The AGNs tend to have higher bulge prominences, redder colours, and higher stellar masses than their star-forming counterparts, although the ranges of these parameters do not vary significantly. The differences between the bar strengths are more apparent in star-forming galaxies than in AGNs, with bulge prominence being particularly divided in undetermined galaxies.

Given that much of the literature indicates a relationship between an AGN and the galactic bulge (e.g. through scaling relations; see Kormendy & Ho 2013 for a review), we investigated how the AGN fraction changes with bulge prominence for each bar strength. Using the sample described in Sect. 2, we controlled only for mass and colour as described above, using ten bins for each. We did not control for bulge prominence, since we wanted to investigate how the AGN fraction changes with bulge prominence. We divided our mass- and colour-controlled sample into ten B bins such that each bin contained the same number of (weighted) galaxies. Within each of these bins, we calculated the AGN fraction in strongly barred, weakly barred, and unbarred galaxies. The results are shown in Fig. 3.

Interestingly, we do see an overall increase in the bar strength of each AGN fraction with bulge prominence; in other words, within a specific bar category, the AGN fraction increases overall with bulge prominence. We also see that within each bulge prominence bin, the AGN fraction increases with bar strength. However, at higher bulge prominences, the picture becomes less clear, with the difference between strong and weak bars fading at around $B \approx 0.45$, and the differences between all bar categories fading around $B \approx 0.6$.

We wanted to ensure that we are not just seeing a trend with stellar mass in Fig. 3, since bulge prominence can vary with stellar mass (e.g. Huertas-Company et al. 2025). To negate the effect of stellar mass, we followed a similar methodology to that used

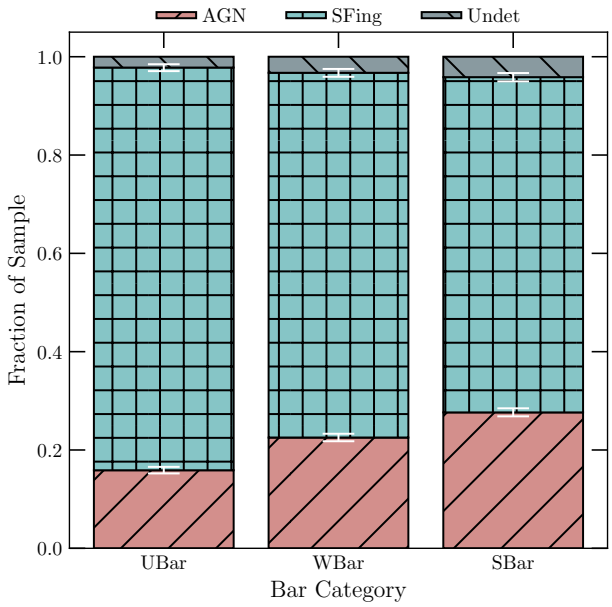

Fig. 2. Fraction of galaxies in each bar strength that are AGNs (red, positive diagonal), star-forming (SFing; teal, square hatching), or undetermined (grey, negative diagonal). Error bars are shown in white. The AGN fraction increases as bar strength increases, although in each case the star-forming fraction is greater than the AGN fraction.

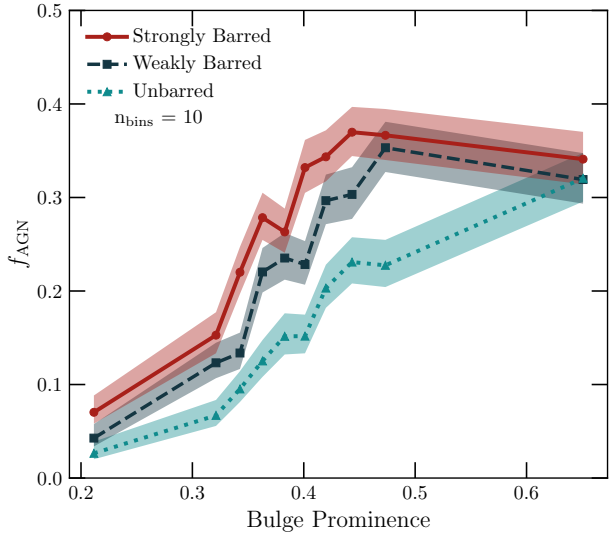

Fig. 3. Effect of bulge prominence on the AGN fraction ($f_{\rm AGN}$) for strongly barred (solid red), weakly barred (dashed navy), and unbarred (dotted teal) disk galaxies. Overall, $f_{\rm AGN}$ increases in each bar strength category with bulge prominence. At lower bulge prominences, $f_{\rm AGN}$ increases in each bulge bin with bar strength; however, the difference between $f_{\rm AGN}$ in strongly and weakly barred galaxies disappears by $B \approx 0.48$, and the difference between all three bar categories disappears around $B \approx 0.6$. The shaded regions show the 1σ uncertainties.

in Masters et al. (2012), although instead of their bar fraction, we used the AGN fraction, and instead of their gas fraction, we used bulge prominence. We show the relationship between bulge prominence and stellar mass for our (uncontrolled) sample in Fig. 4.

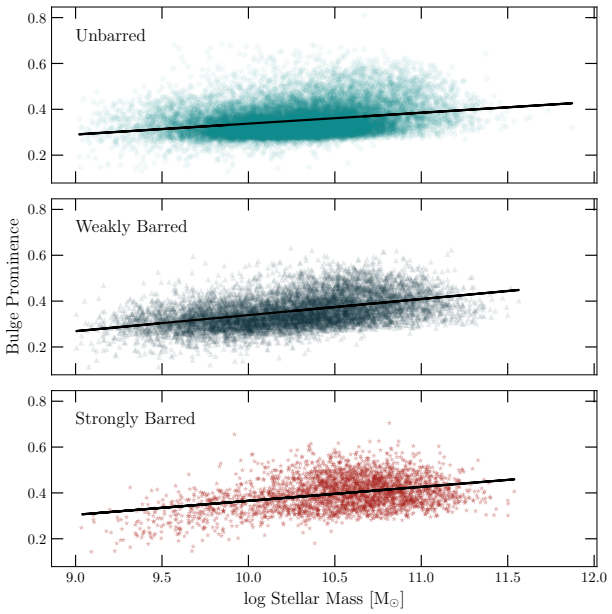

Fig. 4. Relationship between stellar mass and bulge prominence for our sample. Lines of best fit are shown in black. We split the sample by unbarred (teal), weakly barred (navy blue), and strongly barred (red) galaxies. There is a slight increase in the bulge prominence with stellar mass.

Trends are seen for each bar strength. We used linear regression to show that the line of best fit for each bar category is

$$\langle B_{U\rm BAR}\rangle = 0.070\log(M_*/{\rm M}_\odot) - 0.387 \quad (2)$$

$$\langle B_{W\rm BAR}\rangle = 0.077\log(M_*/{\rm M}_\odot) - 0.445 \quad (3)$$

$$\langle B_{S\rm BAR}\rangle = 0.042\log(M_*/{\rm M}_\odot) - 0.058. \quad (4)$$

From here, we could define a measure of bulge surplus, $B_{\rm surp}$, i.e. how much higher a bulge prominence a galaxy has for a given stellar mass,

$$B_{\rm surp} = B - \langle B_{X\rm BAR}\rangle, \quad (5)$$

where XBAR represents the relevant bar category. We then plotted the AGN fraction for each bar strength with the bar surplus using our mass- and colour-controlled sample. The results are shown in Fig. 5.

The horizontal lines show the median $f_{\rm AGN}$ for each bar strength. There is a slight increase in the AGN fraction as the bulge surplus increases. In other words, if the bulge is more prominent than expected for its host galaxy's stellar mass, then there is more likely to be an AGN. This trend is stronger for unbarred than strongly barred galaxies.

We also quantify the difference in bulge surplus for AGN versus inactive galaxies via a Kolmogorov–Smirnov (KS) test (Kolmogorov 1933). The histograms of the bulge surplus distribution are shown in Fig. 6, with p-values for the KS tests written on the plots.

For weakly barred and strongly barred galaxies, the bulge surplus distributions for AGN and inactive galaxies are consistent with being drawn from the same parent sample (2.74σ and 1.97σ, respectively). The unbarred bulge surplus distributions for AGN and inactive galaxies are inconsistent with being drawn from the same parent sample ($>5\sigma$). This indicates that in unbarred galaxies, the excess bulge component is likely linked to AGN presence, but such a bulge component makes less of a difference in barred galaxies. When we limit the redshift to

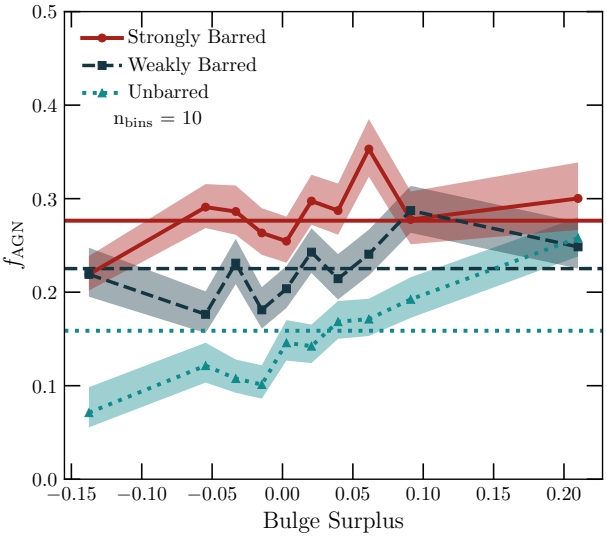

Fig. 5. Variation in f_{AGN} with the bulge surplus, as calculated by Eq. (5), for strongly barred (solid red), weakly barred (dashed navy blue), and unbarred (dotted teal) galaxies. The horizontal lines show the mean f_{AGN} for each bar category. Shaded regions show the 1σ uncertainties. Galaxies at a given stellar mass are more likely to be hosting an AGN if they also have a greater bulge surplus, and this relationship is steeper for unbarred galaxies than for strongly or weakly barred ones.

$z \sim 0.05$, the difference in bulge surplus between the unbarred AGNs and unbarred non-AGNs lessens to $p = 0.08$; however, this is likely due to the significant decrease in the unbarred sample size, by a factor of 5. The p-values for strongly and weakly barred galaxies do not change significantly. Further work with high-resolution images will determine if this is a real trend or a selection effect.

4. Discussion

The positive correlations between the AGN fraction (f_{AGN}) and the bulge prominence (B) and between f_{AGN} and the bar strength in Fig. 3 indicate that there is a highly complex interplay between these three features. There is not only one correlation that mimics the other, and AGN presence correlates with both the bar strength and the bulge prominence even when controlling for the other.

This indicates that AGNs can be triggered and/or fuelled in galaxies both with and without a bulge, with there being a higher AGN fraction in galaxies with a bulge. However, at every bulge prominence, there is a higher AGN fraction in strongly barred galaxies. Similarly, AGNs can be triggered and/or fuelled in galaxies with strong bars, weak bars, or no bars, with there being a higher AGN fraction in strongly barred galaxies. However, at every bar strength, the AGN fraction increases with bulge prominence.

Scaling relations have long demonstrated a link between AGN and bulge properties (i.e. the Häring & Rix 2004 relationship between black hole mass and bulge stellar mass). However, such relations only involve the connection between AGNs that are already switched on, not the presence of the AGN itself. Thus, we know that black hole mass is related to bulge mass, but this does not necessarily mean that bulges are responsible for the switching on of an AGN. Our work shows, however, that the AGN fraction increases with bulge prominence – larger bulges are more likely to host an AGN, indicating that the bulge size (relative to the host galaxy) is linked to AGN switch-on. Note, however, that many of the bulges in our galaxy sample are likely secularly grown, due to the disk-dominated nature of the galaxies.

The relationship between bars and AGNs is less well understood. Recent works, including simulations by Kataria & Vivek (2024) and Frosst et al. (2025) and observations by Silva-Lima et al. (2022) and Garland et al. (2024), indicate that AGNs are more likely to lie in galaxies with a bar, in agreement with our results. However, works such as Goulding et al. (2017, via X-ray-selected AGNs) and Zee et al. (2023, via separate analyses of AGN and non-AGN barred galaxies) show no such correlation. Marels et al. (2025) show that AGNs in barred galaxies are more powerful than those in unbarred galaxies, similar to the scaling relations described above, although they do not discuss AGN presence.

Bars can grow bulges over time via the funnelling of gas into the centre of the galaxy (e.g. Combes 2009). Our results indicate that if a bar is sufficient to grow a bulge component, it is also sufficient to trigger an AGN.

The tapering off of an AGN fraction (i.e. where the graph begins to level out at around 40%) in both of the barred subsamples is likely due to the AGN duty cycle. AGNs seemingly flicker on and off over their lifetimes (Schawinski et al. 2015), so this indicates that the 'on' mode accounts for around 40% of an AGN's total lifetime. The unbarred AGN fraction may also peak around this point at a higher bulge prominence, but we do not have sufficient data to draw solid conclusions on this. The strongly barred galaxies reaching this plateau at a lower B than weakly barred is indicative that strongly barred galaxies are fuelling AGNs more effectively than weakly barred galaxies, which need to build up a higher bulge prominence before triggering AGN switch-on. This could mean that weak bars take longer to trigger an AGN.

We propose the following duty cycle. Assume that there is a galaxy with a disk, no bulge or bar component, and an inactive SMBH at its centre. Such a disk, after some time, forms a bar either through buckling instability or through a tidal interaction (e.g. Hohl 1971; Noguchi 1987; Sellwood & Wilkinson 1993; Skibba et al. 2012). This bar would funnel gas to the centre of the galaxy, triggering an AGN and forming a bulge (e.g. Kormendy & Kennicutt 2004; Athanassoula 2005; Laurikainen et al. 2007; Combes 2009). The stronger the bar is, the more likely it is to trigger the switch-on of an AGN (G24). Simultaneously, the bar can also build up a bulge component, thus meaning that bars that are funnelling enough gas to develop a bulge are also likely to trigger an AGN. If there is a sufficient gas supply, then the bar will allow the bulge to increase in size. At some point, the gas supply runs out and the AGN switches off, leading to a maximum f_{AGN} of around 40%. If the galaxy never develops a bar, its time spent as an AGN that we can detect depends on its bulge strength, but the influence of the bar dominates over this effect, if it is present. Further work will be needed to understand whether such a duty cycle effect is really in operation, including how the AGN fraction varies in barred galaxies over a greater range of redshifts, and whether this effect is stronger in a particular stellar mass regime.

Long-slit spectroscopic data or integral field unit spectra could allow us to measure the ages of the stellar populations in the bar and bulge separately in AGN hosts, rather than relying on the prominence of the bulge as a proxy for the age of the bar. This would help us confirm or rule out the proposed duty cycle. However, such data should be combined with high-resolution

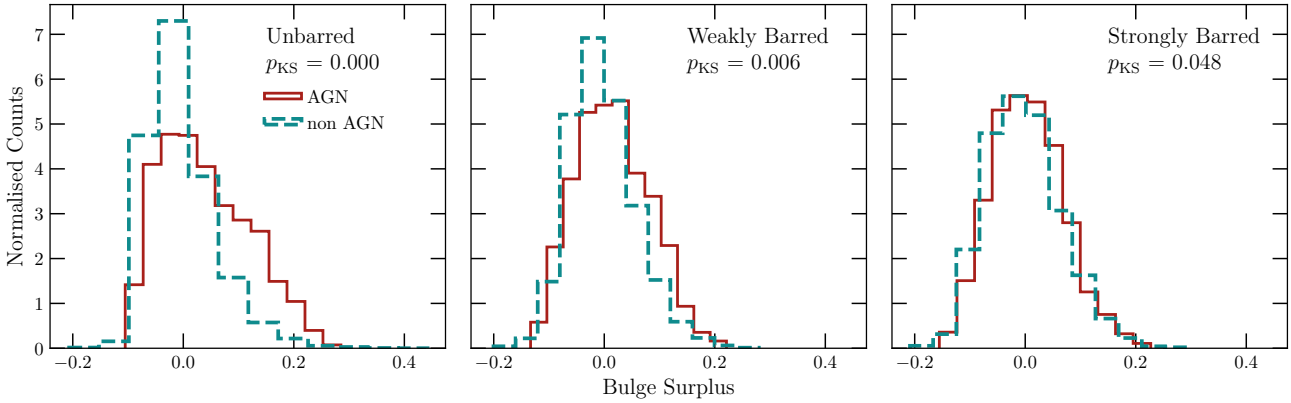

Fig. 6. Normalised distributions of bulge surplus for unbarred (left), weakly barred (centre), and strongly barred (right) galaxies, split between AGN (red) and non-AGN host galaxies (teal). We compare the AGN and non-AGN distributions in each bar category using KS tests, and the p-values are shown on the relevant plots.

imagery such as that from *Euclid* in order to account for other structures, such as nuclear rings and nuclear bars.

The other key reason to consider bar age is that bars are often much longer-lived structures than AGNs: $\sim 10^{9-10}$ yr for bars (Kraljic et al. 2012; Sellwood 2014) compared to $\sim 10^5$ yr for AGN phases (Schawinski et al. 2015). Where we see a barred galaxy without an AGN, it could be that the bar did trigger an AGN that has since switched off. This would be true of other processes as well, and is not just a caveat for studies investigating bar-driven growth.

It is highly important to consider our selection effects when drawing conclusions. The galaxies used in this sample are part of the DESI-LS, which requires that the point-spread function of an image in the z band is a maximum of 1.5 arcsec. At the redshifts of this work ($z \leq 0.1$), this is equivalent to 2.766 kpc. Any bulges or bars smaller than this may not be resolved and thus will remain undetected. Higher-resolution photometry (e.g. from the *Hubble* Space Telescope or *Euclid*) is required to pick out these smaller components and make more accurate morphology classifications. However, despite the limitation on photometry, Fahey et al. (2025) show that samples can be selected from ground-based surveys such as SDSS that are later confirmed to be disk-dominated with *Hubble* Space Telescope photometry.

5. Conclusions

We have used the GZD catalogue first presented in Walmsley et al. (2023b) and the classifications first presented in Garland et al. (2024) to investigate the dual effect of bulge prominence and bar strength on AGN presence. Our key results can be summarised as follows:

- After controlling for bulge prominence, as well as stellar mass and $(g-r)_0$, we find that the AGN fractions in subsamples split by bar strength are in excellent agreement with the results of Garland et al. (2024), who only controlled for stellar mass and $(g-r)_0$. That is to say, strongly barred galaxies have a higher AGN fraction than weakly barred galaxies, which have a higher AGN fraction than unbarred galaxies.
- When we split our controlled sample into bins of bulge prominence, we find the same trends – more strongly barred subsamples have a higher AGN fraction.
- We propose a duty cycle that links the activity of the AGN, bar, and bulge, wherein the bar triggers the AGN to switch on whilst simultaneously building up a bulge.

Further work is required to investigate these AGNs that are fuelled in the absence of bulge components or bar components, as well as investigation of the inactive galaxies where there is a bar and/or bulge present. Integral field unit data, or long-slit spectroscopic data at multiple angles, would allow us to measure the ages of stellar populations in the bar and bulge, as well as measure gas content with respect to the morphological components. Large-scale surveys at high resolutions, such as those being conducted by *Euclid*, would allow for a parametric decomposition of galaxies to a high precision, allowing us to identify bar strengths and bulge prominences to a higher confidence.

Acknowledgements. ILG, HB, MV and MZ have received the support from the Czech Science Foundation Junior Star grant no. GM24-10599M ("Stars in galactic nuclei: interrelation with massive black holes"). LFF acknowledges partial support from NASA Award #80NSSC20M0057. BDS acknowledges support through a UK Research and Innovation Future Leaders Fellowship [grant number MR/T044136/1] and its renewal [grant number MR/Z000076/1]. TG is a Canadian Rubin Fellow at the Dunlap Institute. CJL acknowledges support from the Sloan Foundation. RJS gratefully acknowledges support through the Royal Astronomical Society Research Fellowship. MW is a Dunlap Fellow. The Dunlap Institute is funded through an endowment established by the David Dunlap family and the University of Toronto. The data in this paper are the result of the efforts of the Galaxy Zoo volunteers, without whom none of this work would be possible. Their efforts are individually acknowledged at `http://authors.galaxyzoo.org`. This research has used TOPCAT (Taylor 2005), an interactive graphical tool for analysis and manipulation of tabular data. This research has made extensive use of the following Python packages: ASTROPY, a community-developed core Python package for Astronomy (Astropy Collaboration 2013, 2018, 2022); MATPLOTLIB, a 2D graphics package for Python (Hunter 2007); NUMPY (Harris et al. 2020), a package for scientific computing; SCIPY (Virtanen et al. 2020), a package for fundamental algorithms in scientific computing. Funding for the SDSS and SDSS-II has been provided by the Alfred P. Sloan Foundation, the Participating Institutions, the National Science Foundation, the U.S. Department of Energy, the National Aeronautics and Space Administration, the Japanese Monbukagakusho, the Max Planck Society, and the Higher Education Funding Council for England. The SDSS Web Site is `http://www.sdss.org/`. The SDSS is managed by the Astrophysical Research Consortium for the Participating Institutions. The Participating Institutions are the American Museum of Natural History, Astrophysical Institute Potsdam, University of Basel, University of Cambridge, Case Western Reserve University, University of Chicago, Drexel University, Fermilab, the Institute for Advanced Study, the Japan Participation Group, Johns Hopkins University, the Joint Institute for Nuclear Astrophysics, the Kavli Institute for Particle Astrophysics and Cosmology, the Korean Scientist Group, the Chinese Academy of Sciences (LAMOST), Los Alamos National Laboratory, the Max-Planck-Institute for Astronomy (MPIA), the Max-Planck-Institute for Astrophysics (MPA), New Mexico State University, Ohio State University, University of Pittsburgh, University of Portsmouth, Princeton University, the United States Naval Observatory, and the University of Washington. The Legacy Surveys consist of three individual and complementary projects: the Dark Energy Camera Legacy Survey (DECaLS; Proposal ID #2014B-0404; PIs: David Schlegel and Arjun Dey),

the Beijing-Arizona Sky Survey (BASS; NOAO Prop. ID #2015A-0801; PIs: Zhou Xu and Xiaohui Fan), and the Mayall z-band Legacy Survey (MzLS; Prop. ID #2016A-0453; PI: Arjun Dey). DECaLS, BASS and MzLS together include data obtained, respectively, at the Blanco telescope, Cerro Tololo Inter-American Observatory, NSF's NOIRLab; the Bok telescope, Steward Observatory, University of Arizona; and the Mayall telescope, Kitt Peak National Observatory, NOIRLab. Pipeline processing and analyses of the data were supported by NOIRLab and the Lawrence Berkeley National Laboratory (LBNL). The Legacy Surveys project is honored to be permitted to conduct astronomical research on Iolkam Du'ag (Kitt Peak), a mountain with particular significance to the Tohono O'odham Nation. NOIRLab is operated by the Association of Universities for Research in Astronomy (AURA) under a cooperative agreement with the National Science Foundation. LBNL is managed by the Regents of the University of California under contract to the U.S. Department of Energy. This project used data obtained with the Dark Energy Camera (DECam), which was constructed by the Dark Energy Survey (DES) collaboration. Funding for the DES Projects has been provided by the U.S. Department of Energy, the U.S. National Science Foundation, the Ministry of Science and Education of Spain, the Science and Technology Facilities Council of the United Kingdom, the Higher Education Funding Council for England, the National Center for Supercomputing Applications at the University of Illinois at Urbana-Champaign, the Kavli Institute of Cosmological Physics at the University of Chicago, Center for Cosmology and Astro-Particle Physics at the Ohio State University, the Mitchell Institute for Fundamental Physics and Astronomy at Texas A&M University, Financiadora de Estudos e Projetos, Fundacao Carlos Chagas Filho de Amparo, Financiadora de Estudos e Projetos, Fundacao Carlos Chagas Filho de Amparo a Pesquisa do Estado do Rio de Janeiro, Conselho Nacional de Desenvolvimento Cientifico e Tecnologico and the Ministerio da Ciencia, Tecnologia e Inovacao, the Deutsche Forschungsgemeinschaft and the Collaborating Institutions in the Dark Energy Survey. The Collaborating Institutions are Argonne National Laboratory, the University of California at Santa Cruz, the University of Cambridge, Centro de Investigaciones Energeticas, Medioambientales y Tecnologicas-Madrid, the University of Chicago, University College London, the DES-Brazil Consortium, the University of Edinburgh, the Eidgenossische Technische Hochschule (ETH) Zurich, Fermi National Accelerator Laboratory, the University of Illinois at Urbana-Champaign, the Institut de Ciencies de l'Espai (IEEC/CSIC), the Institut de Fisica d'Altes Energies, Lawrence Berkeley National Laboratory, the Ludwig Maximilians Universitat Munchen and the associated Excellence Cluster Universe, the University of Michigan, NSF's NOIRLab, the University of Nottingham, the Ohio State University, the University of Pennsylvania, the University of Portsmouth, SLAC National Accelerator Laboratory, Stanford University, the University of Sussex, and Texas A&M University. BASS is a key project of the Telescope Access Program (TAP), which has been funded by the National Astronomical Observatories of China, the Chinese Academy of Sciences (the Strategic Priority Research Program "The Emergence of Cosmological Structures" Grant # XDB09000000), and the Special Fund for Astronomy from the Ministry of Finance. The BASS is also supported by the External Cooperation Program of Chinese Academy of Sciences (Grant # 114A11KYSB20160057), and Chinese National Natural Science Foundation (Grant # 12120101003, # 11433005). The Legacy Survey team makes use of data products from the Near-Earth Object Wide-field Infrared Survey Explorer (NEOWISE), which is a project of the Jet Propulsion Laboratory/California Institute of Technology. NEOWISE is funded by the National Aeronautics and Space Administration. The Legacy Surveys imaging of the DESI footprint is supported by the Director, Office of Science, Office of High Energy Physics of the U.S. Department of Energy under Contract No. DE-AC02-05CH1123, by the National Energy Research Scientific Computing Center, a DOE Office of Science User Facility under the same contract; and by the U.S. National Science Foundation, Division of Astronomical Sciences under Contract No. AST-0950945 to NOAO.

References

Abazajian, K. N., Adelman-McCarthy, J. K., Agüeros, M. A., et al. 2009, ApJS, 182, 543
Alonso, S., Coldwell, G., Duplancic, F., Mesa, V., & Lambas, D. G. 2018, A&A, 618, A149
Astropy Collaboration (Robitaille, T. P., et al.) 2013, A&A, 558, A33
Astropy Collaboration (Price-Whelan, A. M., et al.) 2018, AJ, 156, 123
Astropy Collaboration (Price-Whelan, A. M., et al.) 2022, ApJ, 935, 167
Athanassoula, E. 2005, MNRAS, 358, 1477
Baldwin, J. A., Phillips, M. M., & Terlevich, R. 1981, PASP, 93, 5
Beifiori, A., Courteau, S., Corsini, E. M., & Zhu, Y. 2012, MNRAS, 419, 2497
Bell, E. F., Monachesi, A., Harmsen, B., et al. 2017, ApJ, 837, L8
Blanton, M. R., Schlegel, D. J., Strauss, M. A., et al. 2005, AJ, 129, 2562
Cheung, E., Trump, J. R., Athanassoula, E., et al. 2015, MNRAS, 447, 506
Cisternas, M., Jahnke, K., Bongiorno, A., et al. 2011, ApJ, 741, L11
Coelho, P., & Gadotti, D. A. 2011, ApJ, 743, L13
Combes, F. 2009, ASP Conf. Ser., 419, 31
Du, M., Ho, L. C., Debattista, V. P., et al. 2021, ApJ, 919, 135
Fabian, A. 2012, ARA&A, 50, 455
Fahey, M. J., Garland, I. L., Simmons, B. D., et al. 2025, MNRAS, 537, 3511
Ferrarese, L., & Merritt, D. 2000, ApJ, 539, L9
Frosst, M., Obreschkow, D., Ludlow, A., Bottrell, C., & Genel, S. 2025, MNRAS, 537, 3543
Galloway, M. A., Willett, K. W., Fortson, L. F., et al. 2015, MNRAS, 448, 3442
Gargiulo, I. D., Cora, S. A., Vega-Martínez, C. A., et al. 2017, MNRAS, 472, 4133
Garland, I. L., Fahey, M. J., Simmons, B. D., et al. 2023, MNRAS, 522, 211
Garland, I. L., Walmsley, M., Silcock, M. S., et al. 2024, MNRAS, 532, 2320
Géron, T., Smethurst, R. J., Lintott, C., et al. 2021, MNRAS, 507, 4389
Glikman, E., Simmons, B., Mailly, M., et al. 2015, ApJ, 806, 218
Goulding, A. D., Matthaey, E., Greene, J. E., et al. 2017, ApJ, 843, 135
Guo, M., Du, M., Ho, L. C., Debattista, V. P., & Zhao, D. 2020, ApJ, 888, 65
Hamabe, M., & Kormendy, J. 1987, IAU Symp., 127, 379
Häring, N., & Rix, H.-W. 2004, ApJ, 604, L89
Harris, C. R., Millman, K. J., van der Walt, S. J., et al. 2020, Nature, 585, 357
Heckman, T. M., & Best, P. N. 2014, ARA&A, 52, 589
Hinshaw, G., Larson, D., Komatsu, E., et al. 2013, ApJS, 208, 19
Hohl, F. 1971, ApJ, 168, 343
Huertas-Company, M., Shuntov, M., Dong, Y., et al. 2025, A&A, 704, A94
Hunter, J. D. 2007, Comput. Sci. Eng., 9, 90
Kataria, S. K., & Vivek, M. 2024, MNRAS, 527, 3366
Kauffmann, G., Heckman, T. M., Tremonti, C., et al. 2003, MNRAS, 346, 1055
Knapen, J. H., Shlosman, I., & Peletier, R. F. 2000, ApJ, 529, 93
Kolmogorov, A. 1933, Inst. Ital. Attuari Giorn., 4, 83
Kormendy, J. 1977, ApJ, 218, 333
Kormendy, J., & Ho, L. C. 2013, ARA&A, 51, 511
Kormendy, J., & Kennicutt, R. C. 2004, ARA&A, 42, 603
Kormendy, J., Drory, N., Bender, R., & Cornell, M. E. 2010, ApJ, 723, 54
Kraljic, K., Bournaud, F., & Martig, M. 2012, ApJ, 757, 60
La Marca, A., Nardone, M. T., Wang, L., et al. 2026, A&A, 707, A152
Laine, S., Shlosman, I., Knapen, J. H., & Peletier, R. F. 2002, ApJ, 567, 97
Laurikainen, E., Salo, H., & Buta, R. 2004, ApJ, 607, 103
Laurikainen, E., Salo, H., Buta, R., & Knapen, J. H. 2007, MNRAS, 381, 401
Marels, V., Mesa, V., Jaque Arancibia, M., et al. 2025, A&A, 699, A204
Marleau, F. R., Clancy, D., & Bianconi, M. 2013, MNRAS, 435, 3085
Martig, M., Bournaud, F., Croton, D. J., Dekel, A., & Teyssier, R. 2012, ApJ, 756, 26
Martin, G., Kaviraj, S., Volonteri, M., et al. 2018, MNRAS, 476, 2801
Masters, K. L., Nichol, R. C., Haynes, M. P., et al. 2012, MNRAS, 424, 2180
Masters, K. L., Lintott, C. J., Hart, R. E., et al. 2019, MNRAS, 487, 1808
McAlpine, S., Harrison, C. M., Rosario, D. J., et al. 2020, MNRAS, 494, 5713
Noguchi, M. 1987, MNRAS, 228, 635
Oh, S., Oh, K., & Yi, S. K. 2012, ApJS, 198, 4
Park, M.-J., Yi, S. K., Dubois, Y., et al. 2019, ApJ, 883, 25
Parry, O. H., Eke, V. R., & Frenk, C. S. 2009, MNRAS, 396, 1972
Rosario, D. J., Mendel, J. T., Ellison, S. L., Lutz, D., & Trump, J. R. 2016, MNRAS, 457, 2703
Salim, S., Rich, R. M., Charlot, S., et al. 2007, ApJS, 173, 267
Schawinski, K., Koss, M., Berney, S., & Sartori, L. F. 2015, MNRAS, 451, 2517
Sellwood, J. A. 2014, Rev. Mod. Phys., 86, 1
Sellwood, J. A., & Wilkinson, A. 1993, Rep. Progr. Phys., 56, 173
Shlosman, I., Frank, J., & Begelman, M. C. 1989, Nature, 338, 45
Silva-Lima, L. A., Martins, L. P., Coelho, P. R. T., & Gadotti, D. A. 2022, A&A, 661, A105
Simmons, B. D., Smethurst, R. J., & Lintott, C. 2017, MNRAS, 470, 1559
Skibba, R. A., Masters, K. L., Nichol, R. C., et al. 2012, MNRAS, 423, 1485
Smethurst, R. J., Beckmann, R. S., Simmons, B. D., et al. 2024, MNRAS, 527, 10855
Taylor, M. B. 2005, ASP Conf. Ser., 347, 29
Urrutia, T., Lacy, M., & Becker, R. H. 2008, ApJ, 674, 80
Veilleux, S., & Osterbrock, D. E. 1987, ApJS, 63, 295
Virtanen, P., Gommers, R., Oliphant, T. E., et al. 2020, Nat. Meth., 17, 261
Walmsley, M., Lintott, C., Géron, T., et al. 2022, MNRAS, 509, 3966
Walmsley, M., Allen, C., Aussel, B., et al. 2023a, J. Open Source Softw., 8, 5312
Walmsley, M., Géron, T., Kruk, S., et al. 2023b, MNRAS, 526, 4768
Wang, L., Obreschkow, D., Lagos, C. D. P., et al. 2019, MNRAS, 482, 5477
Willett, K. W., Lintott, C. J., Bamford, S. P., et al. 2013, MNRAS, 435, 2835
Zee, W.-B. G., Paudel, S., Moon, J.-S., & Yoon, S.-J. 2023, ApJ, 949, 91

Appendix A: Supplementary stellar mass, colour, and bulge distributions

Figure A.1 shows the stellar mass (M_*), $(g-r)_0$ colour, and bulge prominence (B) distributions for the LINER, composite, and uncertain galaxies in our sample, in a matter identical to Fig. 1.

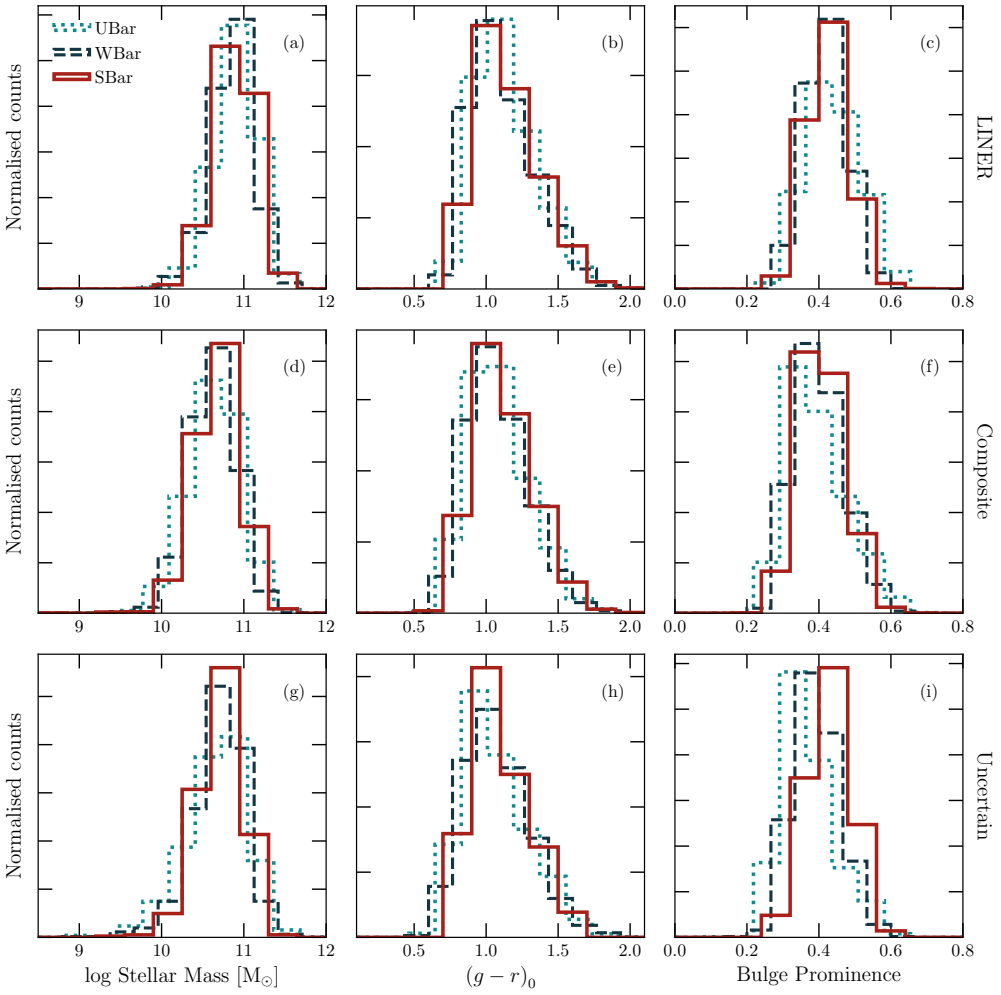

Fig. A.1. Distributions of stellar mass (left column), $(g-r)_0$ colour (middle column), and bulge prominence (right column) for LINER (top row), composite (middle row), and uncertain (bottom row) galaxies. We show strongly barred galaxies in solid red, weakly barred in dashed navy blue, and unbarred in dotted teal.